

1 **Archaeal lipid-inferred paleohydrology and paleotemperature of**  
2 **Lake Chenghai during the Pleistocene-Holocene transition**

3 Weiwei Sun <sup>a</sup>, Enlou Zhang <sup>a,b,\*</sup>, Jie Chang <sup>a</sup>, James Shulmeister <sup>c,d</sup>, Michael I. Bird <sup>e</sup>,  
4 <sup>f</sup>, Cheng Zhao <sup>a,b</sup>, Qingfeng Jiang <sup>g</sup>, Ji Shen <sup>a</sup>

5 <sup>a</sup> State Key Laboratory of Lake Science and Environment, Nanjing Institute of  
6 Geography and Limnology, Chinese Academy of Sciences, Nanjing 210008, China

7 <sup>b</sup> Center for Excellence in Quaternary Science and Global Change, Chinese Academy  
8 of Science, Xian 710061, China

9 <sup>c</sup> School of Earth and Environmental Sciences, The University of Queensland, St  
10 Lucia, Brisbane, Qld, 4072, Australia

11 <sup>d</sup> School of Earth and Environment, University of Canterbury, Private Bag 4800,  
12 Christchurch, New Zealand

13 <sup>e</sup> ARC Centre of Excellence for Australian Biodiversity and Heritage, James Cook  
14 University, PO Box 6811, Cairns, Queensland, 4870, Australia

15 <sup>f</sup> College of Science and Engineering, James Cook University, PO Box 6811, Cairns,  
16 Queensland, 4870, Australia

17 <sup>g</sup> School of Geography Sciences, Nantong University, Nantong, 226007, China

18 \* Corresponding authors. elzhang@niglas.ac.cn. State Key Laboratory of Lake  
19 Science and Environment, Nanjing Institute of Geography and Limnology, Chinese  
20 Academy of Sciences, Nanjing 210008, China

21

22

23

24

25 **ABSTRACT**

26 Over the past decades, paleoenvironmental studies in the Indian Summer  
27 Monsoon (ISM) region have mainly focused on precipitation change, with few  
28 published terrestrial temperature records from the region. We analyzed the distribution  
29 of isoprenoid glycerol dialkyl glycerol tetraethers (isoGDGTs) in the sediments of  
30 Lake Chenghai in southwest China across the Pleistocene–Holocene transition, to  
31 extract both regional hydrological and temperature signals for this important transition  
32 period. Lake-level was reconstructed from the relative abundance of crenarchaeol in  
33 isoGDGTs (%cren) and the crenarchaeol'/crenarchaeol ratio. The %cren-inferred  
34 lake-level identified a single lowstand (15.4-14.4 cal ka BP), while the  
35 crenarchaeol'/crenarchaeol ratio suggests relatively lower lake-level between  
36 15.4-14.4 cal ka BP and 12.5-11.7 cal ka BP, corresponding to periods of weakened  
37 ISM during the Heinrich 1 and Younger Dryas cold event. A filtered TetraEther indeX  
38 consisting of 86 carbon atoms (TEX<sub>86</sub> index) revealed that lake surface temperature  
39 was similar to present-day values during the last deglacial period, and suggests a  
40 substantial warming of ~4 °C from the early Holocene to the mid-Holocene. Our  
41 paleotemperature record is generally consistent with other records in southwest China,  
42 suggesting that the distribution of isoGDGTs in Lake Chenghai sediments has  
43 potential for quantitative paleotemperature reconstruction.

44

45 **Keywords:** Quantitative temperature reconstruction; Lake-level; TEX<sub>86</sub>; Isoprenoid  
46 GDGTs; Lacustrine sediment

47

48

49

50

51

## 52 **1. Introduction**

53 Precipitation variation in the Indian summer monsoon (ISM) region has a great  
54 threat to ecosystem function, water availability and economic security across the  
55 region (Sinha et al., 2011; Sinha et al., 2015; Ljungqvist et al., 2016). This has  
56 stimulated growing scientific interest in understanding the underlying forcing  
57 mechanisms behind climate variability in the ISM region on a range of time-scales, in  
58 order to better predict future monsoonal variations. Over the past two decades, climate  
59 evolution in the ISM region since the Last Glacial Maximum has been reconstructed  
60 from various paleoclimatic archives, including speleothems, and marine/lacustrine  
61 sediments (Dykoski et al., 2005; Rashid et al., 2007; Govil and Divakar Naidu, 2011;  
62 Saraswat et al., 2013; Contreras-Rosales et al., 2014; Wang et al., 2014b; Dutt et al.,  
63 2015; Wu et al., 2015; Kathayat et al., 2016; Zhang et al., 2017a, 2017b; Li et al.,  
64 2018; Zhang et al., 2018; Sun et al., 2019; Zhang et al., 2019). These studies provide  
65 evidence of changes in ISM precipitation on orbital- and millennial time-scales, with  
66 a weakened ISM occurring during cold events, and strengthened ISM occurring  
67 during warm intervals.

68 In addition to precipitation, temperature is an important climatic factor, due to its  
69 significant effects on evaporation and regional hydrological cycle. There remains a  
70 lack of quantitative reconstructions of terrestrial temperature from the ISM region  
71 (Shen et al., 2006; Zhang et al., 2017a; Wu et al., 2018; Feng et al., 2019; Ning et al.,  
72 2019; Tian et al., 2019; Zhang et al., 2019). During the last deglaciation-Holocene  
73 transition, the climate of high latitudes in the Northern Hemisphere is punctuated by  
74 three abrupt, millennial-scale events: the Heinrich 1 (H1) cold event, the  
75 Bølling/Allerød (BA) warm period and the Younger Dryas (YD) cooling (Alley and  
76 Clark, 1999). These intervals are attributed to a variety of mechanisms including  
77 changes to orbitally-controlled insolation, ice sheet extent, oceanic circulation and  
78 atmospheric greenhouse concentrations (Alley and Clark, 1999). The recent  
79 quantitative summer temperature proxy based on pollen and chironomids from  
80 southwest China has been developed to address the response of long-term temperature

81 to the high latitude climate changes (Zhang et al., 2017 and 2019; Wu et al., 2018).  
82 However, the magnitude of these temperature variations is not consistent, and further  
83 studies are required.

84 Glycerol dialkyl glycerol tetraethers (GDGTs) have been widely used for the  
85 quantitative reconstruction of terrestrial paleotemperature during the Quaternary due  
86 to the fact that they are ubiquitous in soils and lacustrine sediments (Blaga et al., 2013;  
87 Wang et al., 2017b; Zheng et al., 2018; Ning et al., 2019; Tian et al., 2019).  
88 Isoprenoid GDGTs (isoGDGTs), comprising acyclic or ring-containing isoprenoidal  
89 biphytanyl carbon chains, are a suit of membrane lipids produced by some species  
90 of archaea, such as Euryarchaeota, Crenarchaeota and Thaumarchaeota (Schouten et  
91 al., 2013). IsoGDGTs containing 0 to 3 cyclopentane moieties (isoGDGTs 0–3, Fig.  
92 S1) are common isoGDGTs with a large range of biological sources (Schouten et al.,  
93 2013). For example, Thaumarchaeota were the dominant biological source of  
94 GDGT-0 in Lake Lucerne from Switzerland (Blaga et al., 2011); while GDGT-0 in  
95 Lake Challa surface sediments might predominantly derive from archaea residing in  
96 the deeper, anoxic water column, such as group 1.2 and marine benthic group C group  
97 of the Crenarchaeota, and the Halobacteriales of the Euryarchaeota (Sinninghe Damsté  
98 et al., 2009); and methanogenic and methanotrophic archaea can also be two  
99 important sources of GDGT-0 within the water column and sediment (Blaga et al.,  
100 2009; Powers et al., 2010). In contrast, crenarchaeol and its regioisomer, crenarchaeol'  
101 (Fig. S1), are considered to be produced specifically by mesophilic Thaumarchaeota  
102 in aquatic environments (Schouten et al., 2002; Blaga et al., 2009; Kim et al., 2010;  
103 Powers et al., 2010; Schouten et al., 2013). On this basis, the ratio of  
104 GDGT-0/crenarchaeol has been proposed to evaluate the influence of Thaumarchaeota  
105 on the distribution of isoGDGTs in lacustrine sediments, and the ratio typically varies  
106 between 0.2 and 2 in Thaumarchaeota (Schouten et al., 2002; Blaga et al., 2009).

107 Thaumarchaeota have a physiological mechanism to increase the weighted  
108 average number of cyclopentane rings in their membrane lipids with growth  
109 temperature (Schouten et al., 2002). Thus the TetraEther indeX consisting of 86

110 carbon atoms (TEX<sub>86</sub> index), which represents the relative number of cyclopentane  
111 moieties in isoGDGT molecules derived from aquatic Thaumarchaeota, has great  
112 potential for use as a paleotemperature proxy in the marine environment and large  
113 lakes (Tierney et al., 2008; Berke et al., 2012; Blaga et al., 2013; Wang et al., 2015).  
114 However, the index may not be a reliable proxy for past temperature in small lakes  
115 due to substantial amounts of soil and/or methanogenic archaea isoGDGTs identified  
116 in the same lacustrine sediment and also due to variability in the depth of isoGDGT  
117 production in aquatic ecosystems (Blaga et al., 2009; Powers et al., 2010; Sinninghe  
118 Damsté et al., 2012a).

119 It has also been shown that crenarchaeol' is only present in low abundance in  
120 most Thaumarchaeota except for the group I.1b Thaumarchaeota, where it is one of  
121 the major isoGDGTs (Kim et al., 2012; Sinninghe Damsté et al., 2012b). The  
122 crenarchaeol'/crenarchaeol ratios for enrichment cultures of group I.1a aquatic  
123 Thaumarchaeota are typically 0.01-0.04, however, for group I.1b Thaumarchaeota  
124 enriched from soils the crenarchaeol'/crenarchaeol ratios are around 0.21 and  
125 substantially higher (Pitcher et al., 2011; Sinninghe Damsté et al., 2012a). In addition,  
126 a likely Group I.1b Thaumarchaeota population inhabiting the subsurface water  
127 column near the anoxic-suboxic boundary was found in Lake Malawi, but the total  
128 production of isoGDGTs by this group appears to be much lower than the  
129 surface-dwelling Thaumarchaeota (Meegan Kumar et al., 2019).

130 In addition, aquatic Thaumarchaeota are nitrifiers, that prefer to live above the  
131 oxycline of relatively deep lakes, as has been observed by a range of lipid biomarker  
132 and DNA based investigations of vertical changes in archaea communities in lake  
133 water columns (Sinninghe Damsté et al., 2009; Blaga et al., 2011; Schouten et al.,  
134 2012; Buckles et al., 2013; Meegan Kumar et al., 2019). Some Thaumarchaeota are  
135 thought to be suppressed by a high light level, which consequently might also inhibit  
136 their ability to thrive near the surface of lakes (Schouten et al., 2013). Further,  
137 Thaumarchaeota are chemoautotrophic and thrive predominantly near the oxycline in  
138 stratified lakes, mainly due to the release of ammonia derived from descending

139 particulate organic matter that is recycled primarily by photoautotrophs or  
140 heterotrophs in the photic zone (Tierney et al., 2010). Consequently, the proportion of  
141 crenarchaeol in isoGDGTs (cren%) has been suggested as lake-level proxy (Wang et  
142 al., 2014a; Wang et al., 2017a; Wang et al., 2019). However, it has also been  
143 suggested that mixing of the water column will be much more frequent at lowstand  
144 conditions, and therefore periodically or permanently oxic, high nutrient availability  
145 water and enhanced nitrogen cycling would be likely to result in a relatively higher  
146 production of crenarchaeol (Filippi and Talbot, 2005; Sinninghe Damst éet al., 2012).

147 In this study, we present an isoGDGT record spanning the last  
148 deglacial-Holocene transition from Lake Chenghai in the southwest China. Our stable  
149 oxygen isotope ( $\delta^{18}\text{O}$ ) record of authigenic carbonates from Lake Chenghai  
150 previously revealed that drought events occurred from 15.6 to 14.4 cal ka BP and 12.5  
151 to 11.7 cal ka BP corresponding to the **H 1** and YD event (Sun et al., 2019). The  
152 present study aims were to (1) identify sources of isoGDGTs in Lake Chenghai  
153 sediments and their linkage, if any, with lake-level variation; (2) test the reliability of  
154 isoGDGT-based proxies as temperature indicators, by comparing our results with  
155 other paleoenvironmental records from adjacent areas, and explore the possible  
156 mechanisms driving temperature variations during the last deglaciation-Holocene  
157 transition in southwestern China.

158

## 159 **2. Materials and methods**

### 160 *2.1. Regional setting*

161 Lake Chenghai (26°27'-26°38'N, 100°38'-100°41'E, Fig. 1A) is a tectonic lake  
162 located in the northwestern part of Yunnan Province (Wang and Dou, 1998). The  
163 current water surface elevation is ~1500 m above sea level (a.s.l.), and the maximum  
164 water depth is ~35 m. The lake is hydrologically closed at present, with a surface area  
165 of ~77 km<sup>2</sup> and a catchment of ~318 km<sup>2</sup> (Wu et al., 2004). However, Lake Chenghai  
166 was linked to the Jinsha River via the Haikou River before a dam at an elevation of

167 ~1540 m a.s.l. was constructed on its southern side at ~0.3 cal ka BP (Wang and Dou,  
168 1998). The annual mean lake surface temperature (LST) is ~16 °C (Wan et al., 2005).  
169 In summer, the lake becomes thermally stratified, with the thermocline at between 10  
170 to 20 m (Fig. 1C, Lu, 2018). Despite a relatively large catchment, the lake level is  
171 mainly maintained by direct precipitation and groundwater, with a total dissolved  
172 solid load of ~1‰ and pH of ~8 (Wan et al., 2005). The lake is eutrophic with a total  
173 phosphate concentration of 0.05 mg/L, and total nitrogen concentration of 0.89 mg/L  
174 (Li et al., 2019). Topsoil types are lateritic red earths and mountain red brown soils in  
175 the catchment (Wang and Dou, 1998). The Lake Chenghai region is mainly affected  
176 by a warm-humid monsoonal airflow from the tropical Indian Ocean from June to  
177 September, and by the southern branch of the Northern Hemisphere westerly jet  
178 between October and May (Wang and Dou, 1998). The mean annual temperature is  
179 ~14 °C, the mean annual precipitation is ~660 mm with 80% falling between June and  
180 September (the Yongsheng meteorological station 26.68°N, 100.75°E; elevation of  
181 2130 m a.s.l.).

## 182 2.2. Sampling and dating

183 In summer 2016, an 874-cm-long sediment core (CH2016) was retrieved using a  
184 UWITEC coring platform system with a percussion corer in 30 m of water depth  
185 (26°33'29.4"N, 100°39'6.7"E). Each section of the core was split lengthways,  
186 photographed and then sectioned at a 1-cm interval in the laboratory; the samples  
187 stored at 4 °C until analysis. The chronology was established using accelerator mass  
188 spectrometry (AMS) <sup>14</sup>C dating of eight terrestrial plant macrofossils and charcoal  
189 (Sun et al., 2019). The radiocarbon analyses were performed at the Beta Analytic  
190 Radiocarbon Dating Laboratory in Miami, USA. The age model was developed  
191 utilizing Bacon, implemented in R 3.1.0 at 5-cm intervals (Blaauw and Andres  
192 Christen, 2011; R Development Core Team, 2013). All AMS <sup>14</sup>C dates were calibrated  
193 to calendar years before present (0 BP =1950) using the program Calib 7.1 and the  
194 IntCal13 calibration data set (Reimer et al., 2013). The basal mean weighted age is  
195 ~15.6 cal ka BP (Fig. 2, Sun et al., 2019).

196 2.3. Lipid extraction and analysis

197 A total of 102 freeze-dried samples at 4-cm interval were collected for GDGT  
198 analysis over the last deglaciation-Holocene transition. The sampling resolution was  
199 increased to 1-cm between 792- 806 cm, due to the low sedimentation rate observed  
200 in this section. In addition, seven surface (the top 2 cm) sediments covering the whole  
201 lake sampled in 2014 were also analyzed. Lipid extraction was undertaken according  
202 to the procedures in Feng et al (2019). A ~4 g aliquot of each sample was extracted  
203 ultrasonically (4 times) with a mixture of dichloromethane and methanol (9:1, v/v).  
204 The supernatants were condensed and saponified at room temperature for 12 h with a  
205 1 M KOH/methanol solution. The neutral fractions were then separated into apolar  
206 and polar fractions on a silica gel column, using *n*-hexane and methanol, respectively.  
207 The polar fraction containing the GDGTs was concentrated and filtered through 0.45  
208  $\mu\text{m}$  polytetrafluoroethylene syringe filters using *n*-hexane/ isopropanol (99:1 v/v), and  
209 then dried under  $\text{N}_2$ .

210 GDGTs were analyzed using an Agilent 1260 series high performance liquid  
211 chromatography-atmospheric pressure chemical ionization-mass spectrometer  
212 (HPLC-APCI-MS), following the procedure of Yang et al. (2015) at the Institute of  
213 Tibetan Plateau Research, Chinese Academy of Sciences. Briefly, the GDGTs were  
214 separated using three silica columns in tandem (100 mm $\times$  2.1 mm, 1.9  $\mu\text{m}$ ; Thermo  
215 Fisher Scientific, U.S.A.), maintained at 40  $^\circ\text{C}$ . The elution gradients were 84%  
216 *n*-hexane (A): 16% ethyl acetate (B) for 5 min, 84/16 to 82/18 A/B for another 60 min,  
217 then to 100% B for 21 min and kept for 4 min, followed by a return to 84/16 A/B for  
218 30 min. The total flow rate of pump A and pump B was maintained at 0.2 ml/min. The  
219 APCI-MS conditions were: vaporizer pressure 60 psi, vaporizer temperature 400  $^\circ\text{C}$ ,  
220 drying gas flow 6 L/min and temperature 200  $^\circ\text{C}$ , capillary voltage 3500 V and corona  
221 current 5  $\mu\text{A}$  (~3200 V). Selected ion monitoring (SIM) mode was performed to target  
222 specific *m/z* values for each GDGT compound, including 1302 (GDGT-0), 1300  
223 (GDGT-1), 1298 (GDGT-2), 1296 (GDGT-3), and 1292 (crenarchaeol and  
224 crenarchaeol'). The results are presented as the fractional of the sum of the isoGDGTs



225 based on the integration of the peak areas of the  $[M+H]^+$  ions.

#### 226 2.4. Index calculation and temperature reconstruction

227 The percentage of each isoGDGT (X) was calculated according to the following  
228 equation:

$$229 \quad \%X = \frac{X}{(\text{GDGT-0} + \text{GDGT-1} + \text{GDGT-2} + \text{GDGT-3} + \text{crenarchaeol} + \text{crenarchaeol}')} \quad (1)$$

231 The  $\text{TEX}_{86}$  index was defined by Schouten et al. (2002) as follows:

$$232 \quad \text{TEX}_{86} = \frac{(\text{GDGT-2} + \text{GDGT-3} + \text{crenarchaeol}')}{(\text{GDGT-1} + \text{GDGT-2} + \text{GDGT-3} + \text{crenarchaeol}')} \quad (2)$$

234  $\text{TEX}_{86}$ -inferred LST was calculated using the global lake calibration of  
235 Castañeda and Schouten (2015):

$$236 \quad \text{LST} = 49.03 \times \text{TEX}_{86} - 10.99 \quad (r^2 = 0.88, n=16, \text{RMSE} = 3.1 \text{ } ^\circ\text{C}) \quad (3)$$

237

### 238 3. Results

239 The isoGDGT compositions varied greatly in Lake Chenghai sediments. As  
240 illustrated in Fig. 3, GDGT-0 is the most abundant isoGDGT composition of the  
241 surface sediments. The relative abundance of GDGT-0 (%GDGT-0) ranged from 71.6-  
242 94.4 with a mean of 89.2%, the %cren values varied from 3.8- 18.1% with a mean of  
243 7.6%. The ratios of GDGT-0/crenarchaeol were from 4.0-24.5 with a mean of 15.5.  
244 The average values of GDGT-1, GDGT-2 and GDGT-3 relative abundance were 1.2,  
245 1.1 and 1.4%, respectively. The crenarchaeol's regioisomer, crenarchaeol', occurred in  
246 only low abundance, close to the detection limit, and therefore  $\text{TEX}_{86}$  values could  
247 not be calculated for these surface sediments.

248 The %cren values ranged between 2.4-61.3% with a mean of 52.4% in the core  
249 CH2016. The %cren values were relatively low and highly variable during 15.4-14.4  
250 cal ka BP, ranging between 1.8-32.0%, with a mean of 11.6%. By contrast, the values

251 were relatively stable during 14.4-7.0 cal ka BP, ranging between 41.8-61.3% with a  
252 mean of 58.3%. The relative abundances of crenarchaeol' had a mean of 1.7%. The  
253 ratios of crenarchaeol'/crenarchaeol were highly variable during 15.4-14.4 cal ka BP  
254 with a mean of 0.07. After this time, the values gradually decrease during 14.4-11.7  
255 cal ka BP time interval with a minor increase between 12.5-11.7 cal ka BP, where the  
256 ratio averaged 0.05. The crenarchaeol'/crenarchaeol ratios were generally stable and  
257 fluctuated around 0.03 during the period 11.8-7.0 cal ka BP.

258 The relative abundances of GDGT-0 (%GDGT-0) showed a significant negative  
259 correlation with the %cren in the core CH2016 ( $r= 0.99$ ,  $p< 0.001$ ). The %GDGT-0  
260 values had a mean of 74.0% between 15.4-14.4 cal ka BP and a mean of 19.6% during  
261 the 14.4-7.0 cal ka BP interval. The values of GDGT-0/crenarchaeol were  
262 generally  $>2$  during the period 15.4-14.4 cal ka BP, ranging from 1.4-49.9 with a  
263 mean of 16.7, and all  $<2$  from 14.4-7.0 cal ka BP. The relative abundance of GDGT-1,  
264 GDGD-2 and GDGT-3 were generally low in the sediments, with means of 8.9, 9.2,  
265 and 1.3, respectively.

266 The  $TEX_{86}$  values were also highly variable during 15.4-14.4 cal ka BP period,  
267 ranging between 0.36-0.68 with a mean of 0.54. Thereafter, the values generally  
268 followed an increasing trend, ranging between 0.49-0.63 with a mean of 0.58.

269

## 270 **4. Discussion**

### 271 *4.1. Provenance of isoGDGTs*

272 In order to evaluate the potential sources of isoGDGTs in Lake Chenghai  
273 sediments, we plotted a ternary diagram to compare the distribution patterns of  
274 GDGT-0, crenarchaeol, and the sum of GDGT-1, GDGT-2, GDGT-3, and  
275 crenarchaeol' (' $TEX_{86}$ ' GDGT) among our samples, previously published Chinese  
276 soils and global marine sediments compiled by Yao et al. (2019), along with  
277 previously published Chinese lacustrine surface sediments results (Günther et al.,  
278 2014; Dang et al., 2016; Hu et al., 2016; Li et al., 2016, 2019; Yao et al., 2019; Wang

279 et al., 2020). In Lake Chenghai surface sediments, GDGT-0 is the predominant  
280 component among the isoGDGTs, consistent with most previous studies of lacustrine  
281 sediments (Blaga et al., 2009; Dang et al., 2016; Li et al., 2019; Yao et al., 2019;  
282 Wang et al., 2020). For example, GDGT-0 can account for more than 90% of total  
283 isoGDGTs in shallow lake surface sediments from East China (Dang et al., 2016); ~80%  
284 in saline pond surface sediments from northeast China (Li et al., 2019), and ~54% in  
285 surface sediments from the Qinghai-Tibetan Plateau (Wang et al., 2020). The values  
286 of GDGT-0/cren >2 in Lake Chenghai surface sediment suggest non-thaumarchaeotal  
287 isoGDGTs are also likely to be an important source in this lake system. The  
288 distribution of isoGDGTs between Chinese lacustrine surface sediments and soils  
289 were similar, and both were generally higher than that in global marine sediments and  
290 Thaumarchaeota. This line of evidence also suggests that the surface sediments could  
291 contain a significant contribution of soil isoGDGTs input (Li et al., 2016; Li et al.,  
292 2019).

293 The distribution of isoGDGT in Lake Chenghai sediment from 15.4-14.4 cal ka  
294 BP was similar to that of the surface sediments, suggesting a substantial contribution  
295 of non-thaumarchaeota during this period. However, the relative abundance of  
296 GDGT-0 significantly decreased and %cren increased in Lake Chenghai sediments  
297 from 14.4-7.0 cal ka BP. The plots generally overlapped with those of global marine  
298 sediments and Thaumarchaeota in the ternary diagram during this period, indicating  
299 that Thaumarchaeota dominated the archaea community in Lake Chenghai during the  
300 late glacial period and the early Holocene. The observed down-core changes in  
301 crenarchaeol'/crenarchaeol ratios may be due to relatively high contributions of group  
302 I.1b Thaumarchaeota from soils during the period 15.4-11.8 cal ka BP, and that these  
303 dominate the contributions of isoGDGTs derived from aquatic group I.1a  
304 Thaumarchaeota during the period from 11.8-7.0 cal ka BP.

#### 305 *4.2. Assessment of isoGDGT-based lake-level proxy*

306 The environmental implication of %cren at Lake Chenghai during the period  
307 from the last deglaciation to the early Holocene is illustrated in Fig. 5. The relatively

308 low %cren values during 15.4-14.4 cal ka BP is consistent in timing with the  $\delta^{18}\text{O}$   
309 record of authigenic carbonates derived from the same core (Fig. 4e, Sun et al., 2019),  
310 speleothem  $\delta^{18}\text{O}$  records from Mawmluh Cave and Bittoo Cave in north India (Fig. 4f,  
311 Dutt et al., 2015; Kathayat et al., 2016), and Donnge Cave in southwest China  
312 (Dykoski et al., 2005), which all record a substantial positive shift in  $\delta^{18}\text{O}$  values at  
313 that time. Speleothem  $\delta^{18}\text{O}$  records in the ISM region are used as a rainfall amount  
314 proxy, tracking changes in monsoon intensity (Dykoski et al., 2005; Cheng et al.,  
315 2012; Dutt et al., 2015). This suggests that the Thaumarchaeota were mainly  
316 suppressed by non-thaumarchaeotal archaea. Thus the abrupt increase in %cren values  
317 at 14.4 cal ka BP is suggested to represent a lowstand of Lake Chenghai during  
318 15.4-14.4 cal ka BP, and a highstand period thereafter.

319 The interpretation of %cren contradicts the case for Lake Challa, but is  
320 consistent with that for Lake Qinghai in northwest China (Sinninghe Damsté et al.,  
321 2012; Wang et al., 2014). This difference is possibly due to the different response of  
322 Thaumarchaeota in the two types of lakes because of the mixing regime. For the small  
323 and deep Lake Challa, there is never complete mixing due to the stable stratification  
324 of the warmer water column and the lack of seasonality (Sinninghe Damsté et al.,  
325 2009). Below the oxycline nitrate levels are high, more substantial mixing regenerates  
326 more nutrients to the surface waters, resulting a relatively higher production of  
327 crenarchaeol (Sinninghe Damsté et al., 2012). In contrast, Lake Chenghai and Lake  
328 Qinghai are seasonal mixing lakes, and the vertical change of nutrients may be  
329 relatively small in the lake water. In addition, the low lake level during the H1 event  
330 was associated with a weakened ISM, and less terrestrial nutrient input due to less  
331 runoff would likely suppress the growth of Thaumarchaeota and reduce the  
332 production of crenarchaeol.

333 Low lake-levels and a weakened ISM during the H1 cold event are also observed  
334 in several previous paleolimnological studies from the Yunnan Plateau, within the  
335 uncertainties of the age model. Diatom and grain-size records from Lake  
336 Tengchongqinghai show a significant decrease in acidophilous diatom species and an

337 increase in the grain-size of mineral particles from 18.5 to 15.0 cal ka BP, suggesting  
338 that the climate was dry and the ISM was at its weakest since the last deglaciation  
339 (Fig. 4g, Zhang et al., 2017b; Li et al., 2018). Similarly, an increase in >30  $\mu\text{m}$   
340 grain-size particles in the late glacial sediments from Lake Xingyun reflects a period  
341 of abrupt weakening of the ISM during the H1 cold event because of reduced lake  
342 level (Wu et al., 2015). In Lake Lugu, the loss of the planktonic diatoms and a switch  
343 to small *Fragilaria* spp. suggests a weaker stratification from 24.5 to 14.5 cal ka BP,  
344 which might also correspond to low lake-level at that time (Wang et al., 2014b). In  
345 addition, there is a peak of cren% centered at ~15.2 cal ka BP, suggesting a centennial  
346 high lake-level and strengthened ISM period, which was not identified in a previous  
347  $\delta^{18}\text{O}$  record of authigenic carbonates (Sun et al., 2019). However, the strengthened  
348 ISM event at ~15.2 cal ka BP was clearly recorded by speleothem  $\delta^{18}\text{O}$  record from  
349 Dongge Cave in southwest China (Dykoski et al., 2005).

350 Lake levels inferred from %cren do not show a lowstand during the YD  
351 (~12.8-11.7 cal ka BP), which is generally recognised as a period of low rainfall due  
352 to the weakening of the ISM (Dutt et al., 2015; Dykoski et al., 2005; Kathayat et al.,  
353 2016; Sun et al., 2019). In contrast, a low lake-level signal is observed in the  $\delta^{18}\text{O}$   
354 record of authigenic carbonates from Lake Chenghai (Sun et al., 2019). In addition,  
355 increased lake water alkalinity and decreased lake-level are also recorded in the  
356 diatom and grain-size proxy records between 12.8-11.1 cal ka BP of Lake  
357 Tengchongqinghai (Fig. 4g, Zhang et al., 2017b; Li et al., 2018). The inferred high  
358 lake levels during the YD which is inconsistent with a weakened ISM inferred from  
359 other proxies, might be due to the erosion of soil organic matter into the lake during  
360 this period (Wang et al., 2019). The crenarchaeol are relatively abundant in topsoils  
361 from southwest China, and the influence of soil input should be more significant at  
362 times of drier conditions (Yang et al., 2019). It is also worth noting that the  
363 crenarchaeol'/crenarchaeol ratios were not only relatively higher during the H1 cold  
364 event, but also showed a minor reversal during the YD cold event. These results are  
365 consistent with group I.1b Thaumarchaeota being an important source of isoGDGTs

366 in small lakes and in the nearshore areas of large lakes (Wang et al., 2019).

367 Another possibility for the unexpected H1 and YD lake level is the sensitivity of  
368 the proxy to lake-level variation in the case of Lake Chenghai. The  $\delta^{18}\text{O}$  record of  
369 authigenic carbonates from Lake Chenghai and speleothem  $\delta^{18}\text{O}$  records in the ISM  
370 region suggest that the weakening of the ISM during the YD was less marked than  
371 that occurring during the H1 event, in turn suggesting that lake-levels in southwest  
372 China may have been higher during the YD than the H1 event (Dykoski et al., 2005;  
373 Dutt et al., 2015; Kathayat et al., 2016; Sun et al., 2019; Zhang et al., 2019). For  
374 the %cren proxy, we note that the values are correlated to the logarithm of depth,  
375 suggesting that %cren may be less sensitive to water depth variation when the  
376 lake-level is relatively high, and more sensitive to water depth variation when the  
377 lake-level is lower (Wang et al., 2019).

#### 378 4.3. Warming in the last deglaciation-Holocene transition

379 The application of the  $\text{TEX}_{86}$ -based paleotemperature calibration depends  
380 critically on the assumption that the isoGDGTs used for calculation of  $\text{TEX}_{86}$  values  
381 are mainly been derived from group I.1a in the water column (Blaga et al., 2009;  
382 Castañeda and Schouten, 2011; Powers et al., 2010; Sinninghe Damsté et al., 2012a).  
383 Since the influence of methanogenic archaea in the water column or archaea in the  
384 catchment soils has been recognized as significant, Lake Chenghai sediments with  
385 crenarchaeol'/crenarchaeol ratios  $>0.04$  and/or GDGT-0/crenarchaeol ratio  $>2$  are  
386 excluded from the discussion below (Powers et al., 2010; Castañeda and Schouten,  
387 2015). The ratio of branched GDGTs to isoGDGTs should be  $<0.5$  if the  
388  $\text{TEX}_{86}$ -temperature calibration in previous studies, because the values are  
389 generally  $>0.90$  in soils, whereas values are close to zero for sediments from large  
390 lakes (Hopmans et al., 2004; Weijers et al., 2006). However, recent studies of a wide  
391 variety of lakes have suggested that at least some of the branched GDGTs can be  
392 produced *in situ* in the lake (Blaga et al., 2010; Tierney et al., 2010; Pearson et al.,  
393 2011; Hu et al., 2016; Dang et al., 2018; Russell et al., 2018). Therefore, *in situ*  
394 production of branched GDGTs in Lake Chenghai cannot be fully excluded, and

395 therefore the ratio of branched GDGTs to isoGDGTs was ignored in this study. 74  
396 samples remain that have isoGDGT distributions consistent with their dominant  
397 source being the aquatic Thaumarchaeota, most of these being from the time interval  
398 between 11.7-7.0 cal ka BP, and only a few from the last deglaciation (n= 6). Using  
399 Equation 4 developed by Castañeda and Schouten (2015) to calculate mean LST,  
400 yielded LST values from 14.3-20.1 °C, with a mean of 18.0 °C (Fig. 5a).

401 LST was ~15.9 °C during the last deglacial period, a temperature approaching  
402 the 16 °C observed in the present Lake Chenghai. Considering the TEX<sub>86</sub>-based  
403 LST transfer function has a RMSE of 3.1 °C, this result is consistent with other recent  
404 reconstructed mean annual temperatures (MAT) in southwest China, which show the  
405 temperatures during the last deglaciation were generally similar to the present-day  
406 values. For example, the MAT inferred from branched GDGTs from Lake  
407 Tengchongqinghai in southwest China increased episodically from 12.0 °C to 14.0 °C  
408 between 19.2 and 10.0 cal ka BP, where the modern mean annual temperature is  
409 14.7 °C (Tian et al., 2019). The TEX<sub>86</sub>-based deglacial LST and MAT inferred from  
410 branched GDGTs from Nam Co in south Tibetan Plateau also reported values similar  
411 to the present-day (Günther et al., 2015). Furthermore, the July temperature derived  
412 from the chironomid record from Lake Tiancai, and pollen record from Lake Yidun  
413 showed that the climate during the deglacial period was ~2-3 °C cooler relative to  
414 today (Fig. 5b and c, Shen et al., 2006; Zhang et al., 2019). The amplitudes of  
415 reconstructed terrestrial temperatures change in the Indian summer monsoon region  
416 are generally consistent with those from the tropical Indian Ocean. Although estimates  
417 of sea surface temperatures in the Andaman Sea and Bay of Bengal were variable, the  
418 cooling ranged from 1-4 °C (Rashid et al., 2007; MARGO, 2009; Govil and Naidu,  
419 2011; Gebregiorgis et al., 2016).

420 Following the YD cold event, LST ranged from 16.2 °C to 20.1 °C with an  
421 increasing trend, and the middle Holocene was generally warmer than the early  
422 Holocene (11.7- 8.2 cal ka BP). In the Indian summer monsoon region, the  
423 reconstructed MAT using the branched GDGT calibration from Lake Ximenglongtan

424 remained at  $\sim 12.5$  °C from 9.4-7.6 cal ka BP, then experienced a rapid warming to  
425  $13.8$  °C from 7.6-5.5 cal ka BP (Ning et al., 2019). Meanwhile, the branched  
426 GDGTs-MAT from Lake Tengchongqinghai also achieved its highest the highest  
427 value at around 7.1 cal ka BP (Tian et al., 2019). Similarly, summer temperatures  
428 reconstructed from Lake Tiancai and Lake Xingyun displayed lower values in the  
429 early Holocene when compared with that in the following millennium, though the  
430 amplitude of change is much lower ( $0.3$  and  $1.1$  °C lower, respectively, Zhang et al.,  
431 2017a; Wu et al., 2018). The amplitude of the absolute scale of cooling and warming  
432 is of a lower magnitude in the chironomid, pollen and branched GDGT records as  
433 compared to the TEX<sub>86</sub>-based reconstruction from Lake Chenghai. This may be due to  
434 the difference in the accuracy and precision of the proxy-based models, which also  
435 depend on the biological and seasonal sensitivity of the proxy, to constrain the  
436 absolute temperature values (Zhang et al., 2017).

437 We also noted that most of the lake records from not only the Indian summer  
438 monsoon region, but other parts of East Asia, show a thermal optimum at  
439 8.0-7.0 cal ka BP (Ning et al., 2019). The summer isolation over the Northern  
440 Hemisphere, which is an important external forcing, was highest at  $\sim 11.0$  cal ka BP,  
441 leading the temperature optimum in east and south Asia by 3-4 ka (Berger and Loutre,  
442 1991). This indicates that additional feedback between solar insolation and internal  
443 processes, such as the persistence of remnants of the Northern Hemisphere ice-sheets  
444 during the early Holocene, should be considered in explaining this discrepancy (Ning  
445 et al., 2019). The Laurentide and Fennoscandian ice-sheets in the early Holocene  
446 enhanced surface albedo and reduced air temperature in the high latitudes, which  
447 likely led to enhanced westerlies transporting more cold air from the North Atlantic  
448 Ocean downward to the Indian monsoon affected regions of southwest China and  
449 north India through its south branch flow (Ning et al., 2019). In addition, the melting  
450 of ice-sheets is likely to have slowed down the Atlantic Meridional Overturning  
451 Circulation. This process could further result in a relatively weakened Indian summer  
452 monsoon, and a reduction in heat transported to the continent during the early



453 Holocene (Zhang et al., 2017a).

454

## 455 **5. Conclusions**

456 The record of isoGDGTs in the sediments of Lake Chenghai in southwest China  
457 presented in this study allows us to test the ability of isoGDGT-based proxies in the  
458 ISM region to reconstruct lake-level and temperature during the last  
459 deglaciation-Holocene transition. The lake-level history inferred from %cren shows a  
460 relative lowstand of Lake Chenghai during 15.4-14.4 cal ka BP, corresponding to a  
461 period of weakened ISM during the H1 cold event. The indistinct signal of lake-level  
462 variation during the YD cold event may be due to the group I.1b Thaumarchaeota  
463 being an important source of isoGDGTs and consequently the lake level may have  
464 been low during the YD cold event. After filtering for the influence of isoGDGTs  
465 derived from soils in the surrounding catchment and non-thaumarchaeota, the TEX<sub>86</sub>  
466 paleothermometry revealed that the LST of Lake Chenghai was similar to the  
467 present-day value during the last deglaciation. The lake also experienced a substantial  
468 warming of ~4 °C from the early-Holocene to the mid-Holocene due to the melting of  
469 the remnants of the continental ice-sheets in the Northern Hemisphere, which  
470 gradually reduced winter westerly circulation. Overall, our results show that records  
471 of isoGDGTs in Lake Chenghai sediments have potential for quantitative  
472 paleotemperature reconstruction once potential underlying biases are properly  
473 constrained.

474

### 475 **Data availability.**

476 All data in this study will be made available on request.

### 477 **Author contributions.**

478 W.S and E.Z designed the study, W.S performed the fieldwork and lab analysis. W.S  
479 and E.Z led the writing of the paper, J.C, J. S, M.I.B, C.Z, Q.J and J.S contributed to

480 data interpretation and paper writing. All authors contributed to discussions and  
481 writing of the manuscript. The authors declare that they have no competing financial  
482 interests.

### 483 **Competing interests.**

484 The authors declare that they have no conflict of interest.

### 485 **Acknowledgments**

486 We thank Dr. R. Chen and D. Ning for field assistance and laboratory analysis. The  
487 research was supported by the fund from the program of Global Change and  
488 Mitigation (2016YFA0600502), the National Natural Science Foundation of China  
489 (41702183 and 41572337), the Strategic Priority Research Program of Chinese  
490 Academy of Sciences (XDB40010200), and the fund from State Key Laboratory of  
491 Lake Science and Environment (2016SKL003).

492

### 493 **References**

- 494 Alley, R.B., Clark, P.U.: The deglaciation of the northern hemisphere: A global  
495 perspective. *Annu. Rev. Earth Pl. Sc.* 27, 149-182, DOI:  
496 10.1146/annurev.earth.27.1.149, 1999.
- 497 Berger, A., Loutre, M.-F.: Insolation values for the climate of the last 10 million years.  
498 *Quaternary. Sci. Rev.* 10, 297-317: DOI: 10.1016/0277-3791(91)90033-Q, 1991.
- 499 Berke, M.A., Johnson, T.C., Werne, J.P., Schouten, S., Sinninghe Damsté J.S.: A  
500 mid-Holocene thermal maximum at the end of the African Humid Period. *Earth.*  
501 *Planet. Sc. Lett.* 351-352, 95-104, DOI: 10.1016/j.epsl.2012.07.008, 2012.
- 502 Blaauw, M., Andres Christen, J.: Flexible paleoclimate age-depth models using an  
503 autoregressive gamma process. *Bayesian. Anal.* 6, 457-474,  
504 DOI: 10.1214/11-BA618, 2011.
- 505 Blaga, C.I., Reichert, G.-J., Heiri, O., Sinninghe Damsté J.S.: Tetraether membrane  
506 lipid distributions in water-column particulate matter and sediments: a study of  
507 47 European lakes along a north–south transect. *J. Paleolimnol.* 41, 523-540,

508 DOI: 10.1007/s10933-008-9242-2, 2009.

509 Blaga, C.I., Reichart, G.-J., Lotter, A.F., Anselmetti, F.S., Sinninghe Damsté J.S.: A  
510 TEX<sub>86</sub> lake record suggests simultaneous shifts in temperature in Central Europe  
511 and Greenland during the last deglaciation. *Geophys. Res. Lett.* 40, 948-953,  
512 DOI: 10.1002/grl.50181, 2013.

513 Blaga, C.I., Reichart, G.-J., Vissers, E.W., Lotter, A.F., Anselmetti, F.S., Sinninghe  
514 Damsté J.S.: Seasonal changes in glycerol dialkyl glycerol tetraether  
515 concentrations and fluxes in a perialpine lake: Implications for the use of the  
516 TEX<sub>86</sub> and BIT proxies. *Geochim. Cosmochim. Ac.* 75, 6416-6428, DOI:  
517 10.1016/j.gca.2011.08.016, 2011.

518 Blaga, C.I., Reichart, G.J., Schouten, S., Lotter, A.F., Werne, J.P., Kosten, S., Mazzeo,  
519 N., Lacerot, G., Damste, J.S.S.: Branched glycerol dialkyl glycerol tetraethers in  
520 lake sediments: Can they be used as temperature and pH proxies? *Org. Geochem.*  
521 41, 1225-1234, DOI: 10.1016/j.orggeochem.2010.07.002, 2010.

522 Buckles, L.K., Villanueva, L., Weijers, J.W.H., Verschuren, D., Damsté J.S.S.:  
523 Linking isoprenoidal GDGT membrane lipid distributions with gene abundances  
524 of ammonia-oxidizing Thaumarchaeota and uncultured crenarchaeotal groups in  
525 the water column of a tropical lake (Lake Challa, East Africa). *Environ.l*  
526 *Microbiol.* 15, 2445-2462, DOI: 10.1111/1462-2920.12118, 2013.

527 Carlson, A.E., LeGrande, A.N., Oppo, D.W., Came, R.E., Schmidt, G.A., Anslow, F.S.,  
528 Licciardi, J.M., Obbink, E.A.: Rapid early Holocene deglaciation of the  
529 Laurentide ice sheet. *Nature Geosci.* 1, 620-624, DOI: 10.1038/ngeo285, 2008.

530 Castañeda, I.S., Schouten, S.: A review of molecular organic proxies for examining  
531 modern and ancient lacustrine environments. *Quaternary. Sci. Rev.* 30,  
532 2851-2891, DOI: 10.1016/j.quascirev.2011.07.009, 2011.

533 Castañeda, I.S., Schouten, S.: Corrigendum to “A review of molecular organic proxies  
534 for examining modern and ancient lacustrine environments” [*Quat. Sci. Rev.* 30  
535 (2011) 2851–2891]. *Quaternary. Sci. Rev.* 125, 174-176, DOI:  
536 10.1016/j.quascirev.2015.07.020, 2015.

537 Cheng, H., Sinha, A., Wang, X., Cruz, F.W., Edwards, R.L.: The Global

538 Paleomonsoon as seen through speleothem records from Asia and the Americas.  
539 *Clim. Dynam.* 39, 1045-1062, DOI: 10.1007/s00382-012-1363-7, 2012.

540 Contreras-Rosales, L.A., Jennerjahn, T., Tharammal, T., Meyer, V., Lückge, A., Paul,  
541 A., Schefuß, E.: Evolution of the Indian Summer Monsoon and terrestrial  
542 vegetation in the Bengal region during the past 18 ka. *Quaternary. Sci. Rev.* 102,  
543 133-148, DOI: 10.1016/j.quascirev.2014.08.010, 2014.

544 Dang, X., Ding, W., Yang, H., Pancost, R.D., Naafs, B.D.A., Xue, J., Lin, X., Lu, J.,  
545 Xie, S.: Different temperature dependence of the bacterial brGDGT isomers in  
546 35 Chinese lake sediments compared to that in soils. *Org. Geochem.*, DOI:  
547 10.1016/j.orggeochem.2018.02.008, 2018.

548 Dang, X.Y., Xue, J.T., Yang, H., Xie, S.C.: Environmental impacts on the distribution  
549 of microbial tetraether lipids in Chinese lakes with contrasting pH: Implications  
550 for lacustrine paleoenvironmental reconstructions. *Sci. China. Earth. Sci.* 59,  
551 939-950, DOI: 10.1007/s11430-015-5234-z, 2016.

552 Dutt, S., Gupta, A.K., Clemens, S.C., Cheng, H., Singh, R.K., Kathayat, G., Edwards,  
553 R.L.: Abrupt changes in Indian summer monsoon strength during 33,800 to  
554 5500 years B.P. *Geophys. Res. Lett.* 42, 5526-5532, DOI:  
555 10.1002/2015GL064015, 2015.

556 Dykoski, C.A., Edwards, R.L., Cheng, H., Yuan, D., Cai, Y., Zhang, M., Lin, Y., Qing,  
557 J., An, Z., Revenaugh, J.: A high-resolution, absolute-dated Holocene and  
558 deglacial Asian monsoon record from Dongge Cave, China. *Earth. Planet. Sc.*  
559 *Lett.* 233, 71-86, DOI: 10.1016/j.epsl.2005.01.036, 2005.

560 Feng, X., Zhao, C., D'Andrea, W.J., Liang, J., Zhou, A., Shen, J.: Temperature  
561 fluctuations during the Common Era in subtropical southwestern China inferred  
562 from brGDGTs in a remote alpine lake. *Earth. Planet. Sc. Lett.* 510, 26-36, DOI:  
563 10.1016/j.epsl.2018.12.028, 2019.

564 Filippi, M.L., Talbot, M.R.: The palaeolimnology of northern Lake Malawi over the  
565 last 25 ka based upon the elemental and stable isotopic composition of  
566 sedimentary organic matter. *Quaternary. Sci. Rev.* 24, 1303-1328, DOI:  
567 10.1016/j.quascirev.2004.10.009, 2005.

568 Gebregiorgis, D., Hathorne, E.C., Sijinkumar, A.V., Nath, B.N., Nürnberg, D., Frank,  
569 M.: South Asian summer monsoon variability during the last ~54 kyrs inferred  
570 from surface water salinity and river runoff proxies. *Quaternary. Sci. Rev.* 138,  
571 6-15, DOI: 10.1016/j.quascirev.2016.02.012, 2016.

572 Govil, P., Divakar Naidu, P.: Variations of Indian monsoon precipitation during the  
573 last 32 kyr reflected in the surface hydrography of the Western Bay of Bengal.  
574 *Quaternary. Sci. Rev.* 30, 3871-3879, DOI: 10.1016/j.quascirev.2011.10.004,  
575 2011.

576 Günther, F., Thiele, A., Gleixner, G., Xu, B., Yao, T., Schouten, S.: Distribution of  
577 bacterial and archaeal ether lipids in soils and surface sediments of Tibetan lakes:  
578 Implications for GDGT-based proxies in saline high mountain lakes. *Org.*  
579 *Geochem.* 67, 19-30, DOI: 10.1016/j.orggeochem.2013.11.014, 2014.

580 Günther, F., Witt, R., Schouten, S., Mäusbacher, R., Daut, G., Zhu, L., Xu, B., Yao, T.,  
581 Gleixner, G.: Quaternary ecological responses and impacts of the Indian Ocean  
582 Summer Monsoon at Nam Co, Southern Tibetan Plateau. *Quaternary. Sci. Rev.*  
583 112, 66-77, 10.1016/j.quascirev.2015.01.023, 2015.

584 Hu, J., Zhou, H., Peng, P.a., Spiro, B.: Seasonal variability in concentrations and  
585 fluxes of glycerol dialkyl glycerol tetraethers in Huguangyan Maar Lake, SE  
586 China: Implications for the applicability of the MBT-CBT paleotemperature  
587 proxy in lacustrine settings. *Chem. Geol.* 420, 200-212, DOI:  
588 10.1016/j.chemgeo.2015.11.008, 2016.

589 Kathayat, G., Cheng, H., Sinha, A., Spötl, C., Edwards, R.L., Zhang, H., Li, X., Yi, L.,  
590 Ning, Y., Cai, Y., Lui, W.L., Breitenbach, S.F.M.: Indian monsoon variability on  
591 millennial-orbital timescales. *Sci. Rep-UK.* 6, DOI: 10.1038/srep24374, 2016.

592 Kim, J.-G., Jung, M.-Y., Park, S.-J., Rijpstra, W.I.C., Sinninghe Damsté J.S., Madsen,  
593 E.L., Min, D., Kim, J.-S., Kim, G.-J., Rhee, S.-K.: Cultivation of a highly  
594 enriched ammonia-oxidizing archaeon of thaumarchaeotal group I.1b from an  
595 agricultural soil. *Environ. Microbiol.* 14, 1528-1543, DOI:  
596 10.1111/j.1462-2920.2012.02740.x, 2012.

597 Kim, J.-H., van der Meer, J., Schouten, S., Helmke, P., Willmott, V., Sangiorgi, F.,

598 Koç N., Hopmans, E.C., Damsté J.S.S.: New indices and calibrations derived  
599 from the distribution of crenarchaeal isoprenoid tetraether lipids: Implications for  
600 past sea surface temperature reconstructions. *Geochim. Cosmochim. Ac.* 74,  
601 4639-4654, DOI: 10.1016/j.gca.2010.05.027, 2010.

602 Li, J.J., Pancost, R.D., Naafs, B.D.A., Yang, H., Zhao, C., Xie, S.C.: Distribution of  
603 glycerol dialkyl glycerol tetraether (GDGT) lipids in a hypersaline lake system.  
604 *Org. Geochem.* 99, 113-124, DOI: 10.1016/j.orggeochem.2016.06.007, 2016.

605 Li, J., Pancost, R.D., Naafs, B.D.A., Yang, H., Liu, D., Gong, L., Qiu, X., Xie, S.:  
606 Multiple environmental and ecological controls on archaeal ether lipid  
607 distributions in saline ponds. *Chem. Geol.* 529, 119293: DOI:  
608 10.1016/j.chemgeo.2019.119293, 2019.

609 Li, K., Zhou, Y., Zhou, Q., Dong, Y., Zhang, Y., Chang, J., Chen, L., Lu, Y.:  
610 Temporal-spatial distribution of euphotic depth and its influencing factors in  
611 Lake Chenghai, Yunnan Province, China. *J. Lake Sci.* 31 (1), 256-267, DOI: 10.  
612 18307 /2019. 0124, .2019

613 Li, Y., Chen, X., Xiao, X., Zhang, H., Xue, B., Shen, J., Zhang, E.: Diatom-based  
614 inference of Asian monsoon precipitation from a volcanic lake in southwest  
615 China for the last 18.5 ka. *Quaternary. Sci. Rev.* 182, 109-120, DOI:  
616 10.1016/j.quascirev.2017.11.021, 2018.

617 Ling, Y., Sun, Q., Zheng, M., Wang, H., Luo, Y., Dai, X., Xie, M., Zhu, Q.:  
618 Alkenone-based temperature and climate reconstruction during the last  
619 deglaciation at Lake Dangxiong Co, southwestern Tibetan Plateau. *Quatern. Int.*  
620 443, 58-69, DOI: 10.1016/j.quaint.2016.07.036, 2017.

621 Ljungqvist, F.C., Krusic, P.J., Sundqvist, H.S., Zorita, E., Brattström, G., Frank, D.:  
622 Northern Hemisphere hydroclimate variability over the past twelve centuries.  
623 *Nature* 532, 94-98, DOI: 10.1038/nature17418, 2016.

624 Lu Z., Study on climatic and environmental changes of the Yunnan Chenghai region  
625 recorded by lake sediments since 1800 [D]. Kunming: The master Thesis of  
626 Yunnan Normal University, 39-43, 2018.

627 MARGO Project Members: Constraints on the magnitude and patterns of ocean

628 cooling at the Last Glacial Maximum. *Nature Geosci.* 2, 127-132, DOI:  
629 10.1038/ngeo411, 2009.

630 McManus, J.F., Francois, R., Gherardi, J.M., Keigwin, L.D., Brown-Leger, S.:  
631 Collapse and rapid resumption of Atlantic meridional circulation linked to  
632 deglacial climate changes. *Nature* 428, 834-837, DOI: 10.1038/nature02494,  
633 2004.

634 Meegan Kumar, D., Woltering, M., Hopmans, E.C., Sinninghe Damsté J.S., Schouten,  
635 S., Werne, J.P.: The vertical distribution of Thaumarchaeota in the water column  
636 of Lake Malawi inferred from core and intact polar tetraether lipids. *Org.*  
637 *Geochem.* 132, 37-49, DOI: 10.1016/j.orggeochem.2019.03.004, 2019.

638 Ning, D., Zhang, E., Shulmeister, J., Chang, J., Sun, W., Ni, Z.: Holocene mean  
639 annual air temperature (MAAT) reconstruction based on branched glycerol  
640 dialkyl glycerol tetraethers from Lake Ximenglongtan, southwestern China. *Org.*  
641 *Geochem.* 133, 65-76, DOI: 10.1016/j.orggeochem.2019.05.003, 2019.

642 Pearson, E.J., Juggins, S., Talbot, H.M., Weckstrom, J., Rosen, P., Ryves, D.B.,  
643 Roberts, S.J., Schmidt, R.: A lacustrine GDGT-temperature calibration from the  
644 Scandinavian Arctic to Antarctic: Renewed potential for the application of  
645 GDGT-paleothermometry in lakes. *Geochim. Cosmochim. Ac.* 75, 6225-6238,  
646 DOI: 10.1016/j.gca.2011.07.042, 2011.

647 Pitcher, A., Hopmans, E.C., Mosier, A.C., Park, S.-J., Rhee, S.-K., Francis, C.A.,  
648 Schouten, S., Sinninghe Damsté J.S.: Core and Intact Polar Glycerol  
649 Dibiphytanyl Glycerol Tetraether Lipids of Ammonia-Oxidizing Archaea  
650 Enriched from Marine and Estuarine Sediments. *Appl. Environ. Microb.* 77,  
651 3468, DOI: 10.1128/AEM.02758-10, 2011.

652 Powers, L., Werne, J.P., Vanderwoude, A.J., Sinninghe Damsté J.S., Hopmans, E.C.,  
653 Schouten, S.: Applicability and calibration of the TEX<sub>86</sub> paleothermometer in  
654 lakes. *Org. Geochem.* 41, 404-413, DOI: 10.1016/j.orggeochem.2009.11.009,  
655 2010.

656 Powers, L.A., Werne, J.P., Johnson, T.C., Hopmans, E.C., Damsté, J.S.S., Schouten, S.:  
657 Crenarchaeotal membrane lipids in lake sediments: A new paleotemperature

658 proxy for continental paleoclimate reconstruction? *Geology* 32, 613-616, DOI:  
659 10.1130/G20434.1, 2004.

660 R Development Core Team, R: A language and environment for statistical computing,  
661 R Foundation for Statistical Computing, Vienna, Austria, 2013.

662 Rashid, H., Flower, B.P., Poore, R.Z., Quinn, T.M.: A ~25 ka Indian Ocean monsoon  
663 variability record from the Andaman Sea. *Quaternary. Sci. Rev.* 26, 2586-2597,  
664 DOI: 10.1016/j.quascirev.2007.07.002, 2007.

665 Reimer, P.J., Bard, E., Bayliss, A., Beck, J.W., Blackwell, P.G., Ramsey, C.B., Buck,  
666 C.E., Cheng, H., Edwards, R.L., Friedrich, M.: IntCal13 and Marine13  
667 radiocarbon age calibration curves 0–50,000 years cal BP. *Radiocarbon* 55,  
668 1869-1887, DOI: 10.2458/azu\_js\_rc.55.16947, 2013.

669 Russell, J.M., Hopmans, E.C., Loomis, S.E., Liang, J., Sinninghe Damsté J.S.:  
670 Distributions of 5- and 6-methyl branched glycerol dialkyl glycerol tetraethers  
671 (brGDGTs) in East African lake sediment: Effects of temperature, pH, and new  
672 lacustrine paleotemperature calibrations. *Org. Geochem.* 117, 56-69, DOI:  
673 10.1016/j.orggeochem.2017.12.003, 2018.

674 Saraswat, R., Lea, D.W., Nigam, R., Mackensen, A., Naik, D.K.: Deglaciation in the  
675 tropical Indian Ocean driven by interplay between the regional monsoon and  
676 global teleconnections. *Earth. Planet. Sc. Lett.* 375, 166-175, DOI:  
677 10.1016/j.epsl.2013.05.022, 2013.

678 Schouten, S., Hopmans, E.C., Schefuß, E., Sinninghe Damsté J.S.: Distributional  
679 variations in marine crenarchaeotal membrane lipids: a new tool for  
680 reconstructing ancient sea water temperatures? *Earth. Planet. Sc. Lett.* 204,  
681 265-274, DOI: 10.1016/S0012-821X(02)00979-2, 2002.

682 Schouten, S., Hopmans, E.C., Sinninghe Damsté J.S.: The organic geochemistry of  
683 glycerol dialkyl glycerol tetraether lipids: A review. *Org. Geochem.* 54, 19-61,  
684 DOI: 10.1016/j.orggeochem.2012.09.006, 2013.

685 Schouten, S., Rijpstra, W.I.C., Durisch-Kaiser, E., Schubert, C.J., Sinninghe Damsté  
686 J.S.: Distribution of glycerol dialkyl glycerol tetraether lipids in the water  
687 column of Lake Tanganyika. *Org. Geochem.* 53, 34-37, DOI:



688 10.1016/j.orggeochem.2012.01.009, 2012.

689 Shen, C., Liu, K.-b., Tang, L., Overpeck, J.T.: Quantitative relationships between  
690 modern pollen rain and climate in the Tibetan Plateau. *Rev. Palaeobot. Palyno.*  
691 140, 61-77, DOI: 10.1016/j.revpalbo.2006.03.001, 2006.

692 Sinha, A., Kathayat, G., Cheng, H., Breitenbach, S.F.M., Berkelhammer, M.,  
693 Mudelsee, M., Biswas, J., Edwards, R.L.: Trends and oscillations in the Indian  
694 summer monsoon rainfall over the last two millennia. *Nat. Commun.* 6, DOI:  
695 10.1038/ncomms7309, 2015.

696 Sinha, A., Stott, L., Berkelhammer, M., Cheng, H., Edwards, R.L., Buckley, B.,  
697 Aldenderfer, M., Mudelsee, M.: A global context for megadroughts in monsoon  
698 Asia during the past millennium. *Quaternary. Sci. Rev.* 30, 47-62, DOI:  
699 10.1016/j.quascirev.2010.10.005, 2011.

700 Sinninghe Damsté J.S., Ossebaar, J., Abbas, B., Schouten, S., Verschuren, D.: Fluxes  
701 and distribution of tetraether lipids in an equatorial African lake: Constraints on  
702 the application of the TEX<sub>86</sub> palaeothermometer and BIT index in lacustrine  
703 settings. *Geochim. Cosmochim. Ac.* 73, 4232-4249, DOI:  
704 10.1016/j.gca.2009.04.022, 2009.

705 Sinninghe Damsté J.S., Ossebaar, J., Schouten, S., Verschuren, D.: Distribution of  
706 tetraether lipids in the 25-ka sedimentary record of Lake Challa: extracting  
707 reliable TEX<sub>86</sub> and MBT/CBT palaeotemperatures from an equatorial African  
708 lake. *Quaternary. Sci. Rev.* 50, 43-54, DOI: 10.1016/j.quascirev.2012.07.001,  
709 2012a.

710 Sinninghe Damsté J.S., Rijpstra, W.I.C., Hopmans, E.C., Jung, M.-Y., Kim, J.-G.,  
711 Rhee, S.-K., Stieglmeier, M., Schleper, C.: Intact Polar and Core Glycerol  
712 Dibiphytanyl Glycerol Tetraether Lipids of Group I.1a and I.1b *Thaumarchaeota*  
713 in Soil. *Appl. Environ Microb* 78, 6866-6874, DOI: 10.1128/AEM.01681-12,  
714 2012b.

715 Sun, W., Zhang, E., Shulmeister, J., Bird, M.I., Chang, J., Shen, J.: Abrupt changes in  
716 Indian summer monsoon strength during the last deglaciation and early Holocene  
717 based on stable isotope evidence from Lake Chenghai, southwest China.

718 Quaternary. Sci. Rev. 218, 1-9, DOI: 10.1016/j.quascirev.2019.06.006, 2019.

719 Tian, L., Wang, M., Zhang, X., Yang, X., Zong, Y., Jia, G., Zheng, Z., Man, M.:  
720 Synchronous change of temperature and moisture over the past 50 ka in  
721 subtropical southwest China as indicated by biomarker records in a crater lake.  
722 Quaternary. Sci. Rev. 212, 121-134, DOI: 10.1016/j.quascirev.2019.04.003,  
723 2019.

724 Tierney, J.E., Russell, J.M., Huang, Y., Damst é J.S.S., Hopmans, E.C., Cohen, A.S.:  
725 Northern Hemisphere controls on tropical southeast African climate during the  
726 past 60,000 years. Science 322, 252-255, DOI: 10.1126/science.1160485, 2008.

727 Tierney, J.E., Russell, J.M., Eggermont, H., Hopmans, E.C., Verschuren, D., Damste,  
728 J.S.S.: Environmental controls on branched tetraether lipid distributions in  
729 tropical East African lake sediments. Geochim. Cosmochim. Ac. 74, 4902-4918,  
730 DOI: 10.1016/j.gca.2010.06.002, 2010.

731 Wan, G.J., Chen, J.A., Wu, F.C., Xu, S.Q., Bai, Z.G., Wan, E.Y., Wang, C.S., Huang,  
732 R.G., Yeager, K.M., Santschi, P.H.: Coupling between <sup>210</sup>Pb<sub>ex</sub> and organic matter  
733 in sediments of a nutrient-enriched lake: An example from Lake Chenghai, China.  
734 Chem Geol 224, 223-236, DOI: 10.1016/j.chemgeo.2005.07.025, 2005.

735 Wang, H., Dong, H., Zhang, C.L., Jiang, H., Liu, Z., Zhao, M., Liu, W.: Deglacial and  
736 Holocene archaeal lipid-inferred paleohydrology and paleotemperature history of  
737 Lake Qinghai, northeastern Qinghai–Tibetan Plateau. Quaternary. Res. 83,  
738 116-126, DOI: 10.1016/j.yqres.2014.10.003, 2015.

739 Wang, H., Dong, H., Zhang, C.L., Jiang, H., Zhao, M., Liu, Z., Lai, Z., Liu, W.: Water  
740 depth affecting thaumarchaeol production in Lake Qinghai, northeastern  
741 Qinghai–Tibetan plateau: Implications for paleo lake levels and paleoclimate.  
742 Chem. Geol. 368, 76-84, DOI: 10.1016/j.chemgeo.2014.01.009, 2014a.

743 Wang, H., He, Y., Liu, W., Zhou, A., Kolpakova, M., Krivonogov, S., Liu, Z.: Lake  
744 Water Depth Controlling Archaeal Tetraether Distributions in Midlatitude Asia:  
745 Implications for Paleo Lake-Level Reconstruction. Geophys. Res. Lett. 46,  
746 5274-5283, DOI: 10.1029/2019GL082157, 2019.

747 Wang, H., Leng, Q., Liu, W., Yang, H.: A rapid lake-shallowing event terminated

748 preservation of the Miocene Clarkia Fossil Konservat-Lagerstätte (Idaho, USA).  
749 *Geology* 45, 239-242, DOI: 10.1130/G38434.1, 2017a.

750 Wang, M., Tian, Q., Li, X., Liang, J., He, Y., Hou, J.: TEX<sub>86</sub> as a potential proxy of  
751 lake water pH in the Tibetan Plateau. *Palaeogeogr. Palaeoclimatol.* 538, 109381, DOI:  
752 10.1016/j.palaeo.2019.109381, 2020.

753 Wang, M., Zheng, Z., Man, M., Hu, J., Gao, Q.: Branched GDGT-based  
754 paleotemperature reconstruction of the last 30,000 years in humid monsoon  
755 region of Southeast China. *Chem. Geol.* 463, 94-102, DOI:  
756 10.1016/j.chemgeo.2017.05.014, 2017b.

757 Wang, Q., Yang, X., Anderson, N.J., Zhang, E., Li, Y.: Diatom response to climate  
758 forcing of a deep, alpine lake (Lugu Hu, Yunnan, SW China) during the Last  
759 Glacial Maximum and its implications for understanding regional monsoon  
760 variability. *Quaternary. Sci. Rev.* 86, 1-12, DOI: 10.1016/j.quascirev.2013.12.024,  
761 2014b.

762 Wang, S., Dou, H.: *Lakes in China*. Science Press, Beijing, China (in Chinese), 1998.

763 Weijers, J.W.H., Schouten, S., Spaargaren, O.C., Damste, J.S.S.: Occurrence and  
764 distribution of tetraether membrane lipids in soils: Implications for the use of the  
765 TEX<sub>86</sub> proxy and the BIT index. *Org. Geochem.* 37, 1680-1693, DOI:  
766 10.1016/j.orggeochem.2006.07.018, 2006.

767 Wu, D., Chen, X., Lv, F., Brenner, M., Curtis, J., Zhou, A., Chen, J., Abbott, M., Yu, J.,  
768 Chen, F.: Decoupled early Holocene summer temperature and monsoon  
769 precipitation in southwest China. *Quaternary. Sci. Rev.* 193, 54-67, DOI:  
770 10.1016/j.quascirev.2018.05.038, 2018.

771 Wu, D., Zhou, A., Chen, X., Yu, J., Zhang, J., Sun, H.: Hydrological and ecosystem  
772 response to abrupt changes in the Indian monsoon during the last glacial, as  
773 recorded by sediments from Xingyun Lake, Yunnan, China. *Palaeogeogr.*  
774 *Palaeoclimatol.* 421, 15-23, DOI: 10.1016/j.palaeo.2015.01.005, 2015.

775 Wu, J., Gagan, M.K., Jiang, X., Xia, W., Wang, S.: Sedimentary geochemical  
776 evidence for recent eutrophication of Lake Chenghai, Yunnan, China. *J.*  
777 *Paleolimnol.* 32, 85-94, 2004.

778 Yao, Y., Zhao, J., Bauersachs, T., Huang, Y.: Effect of water depth on the TEX<sub>86</sub> proxy  
779 in volcanic lakes of northeastern China. *Org. Geochem.* 129, 88-98, DOI:  
780 10.1016/j.orggeochem.2019.01.014, 2019.

781 Yang, H., Xiao, W., Słowakiewicz, M., Ding, W., Ayari, A., Dang, X., Pei, H.:  
782 Depth-dependent variation of archaeal ether lipids along soil and peat profiles  
783 from southern China: Implications for the use of isoprenoidal GDGTs as  
784 environmental tracers. *Org. Geochem.* 128, 42-56, DOI:  
785 <https://doi.org/10.1016/j.orggeochem.2018.12.009>, 2019.

786 Zhang, E., Chang, J., Cao, Y., Sun, W., Shulmeister, J., Tang, H., Langdon, P.G., Yang,  
787 X., Shen, J.: Holocene high-resolution quantitative summer temperature  
788 reconstruction based on subfossil chironomids from the southeast margin of the  
789 Qinghai-Tibetan Plateau. *Quaternary. Sci. Rev.* 165, 1-12, DOI:  
790 10.1016/j.quascirev.2017.04.008, 2017a.

791 Zhang, E., Chang, J., Shulmeister, J., Langdon, P., Sun, W., Cao, Y., Yang, X., Shen, J.:  
792 Summer temperature fluctuations in Southwestern China during the end of the  
793 LGM and the last deglaciation. *Earth. Planet. Sc. Lett.* 509, 78-87, DOI:  
794 10.1016/j.espl.2018.12.024, 2019.

795 Zhang, E., Sun, W., Chang, J., Ning, D., Shulmeister, J.: Variations of the Indian  
796 summer monsoon over the last 30 000 years inferred from a pyrogenic carbon  
797 record from south-west China. *J. Quaternary. Sci.* 33, 131-138, DOI:  
798 10.1002/jqs.3008, 2018.

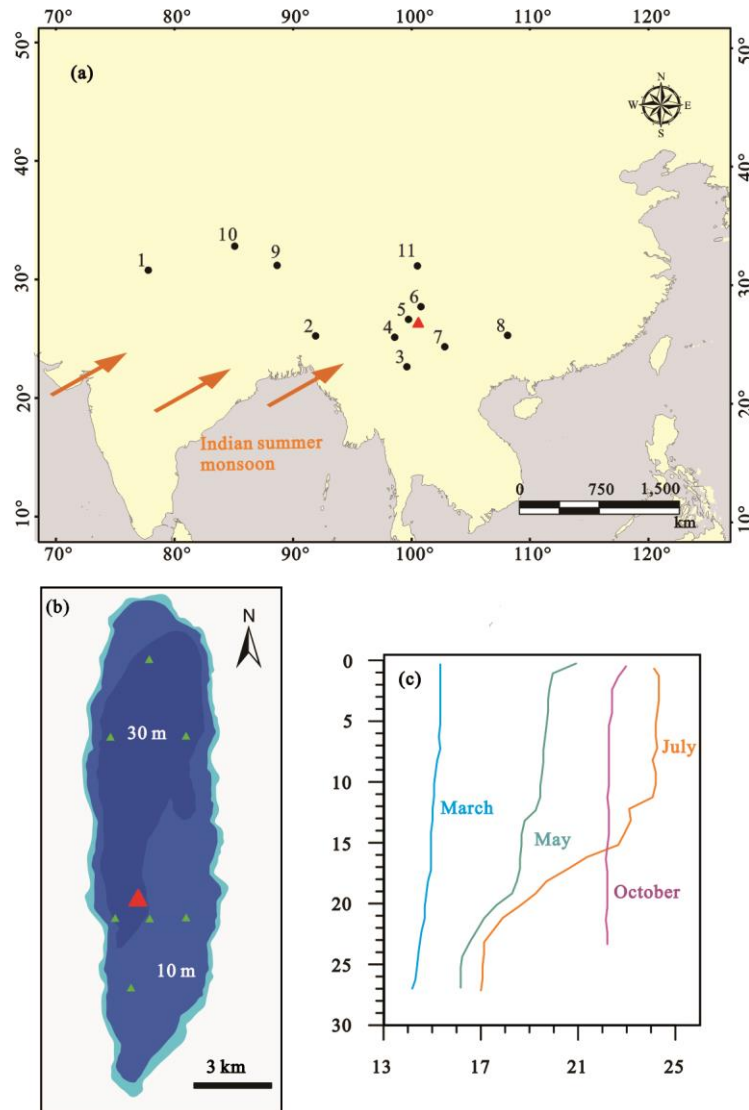
799 Zhang, E., Zhao, C., Xue, B., Liu, Z., Yu, Z., Chen, R., Shen, J.: Millennial-scale  
800 hydroclimate variations in southwest China linked to tropical Indian Ocean since  
801 the Last Glacial Maximum. *Geology* 45, 435-438, DOI: 10.1130/G38309.1,  
802 2017b.

803 Zheng, Y., Pancost, R.D., Naafs, B.D.A., Li, Q., Liu, Z., Yang, H.: Transition from a  
804 warm and dry to a cold and wet climate in NE China across the Holocene. *Earth.*  
805 *Planet. Sc. Lett.* 493, 36-46, DOI: 10.1016/j.epsl.2018.04.019, 2018.

806

807 **Figure captions**

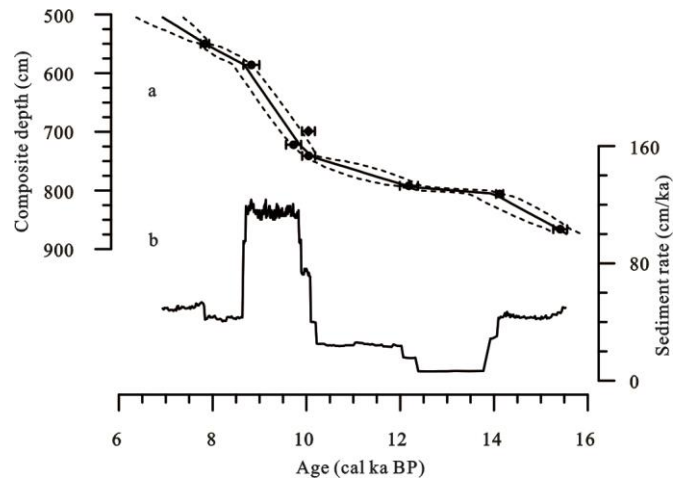
808



809

810 **Fig. 1.** (a) Map showing the location of Lake Chenghai in southwest China (red  
811 triangle) and other sites (circles) mentioned in the text: 1. Bittoo Cave (Kathayat et al.,  
812 2016); 2. Mawmluh Cave (Dutt et al., 2015); 3. Lake Ximenglongtan (Ning et al.,  
813 2019); 4. Lake Tengchongqinghai (Zhang et al., 2017b; Li et al., 2018; Tian et al.,  
814 2019); 5. Lake Tiancai (Zhang et al., 2017a, 2019); 6. Lake Lugu (Wang et al., 2014);  
815 7. Lake Xingyun (Wu et al., 2015, 2018); 8. Dongge Cave (Dykoski et al., 2005); 9.  
816 Nam Co (Günther et al., 2015); 10. Dangxiong Co (Ling et al., 2017); 11. Lake Yidun  
817 (Shen et al., 2006), (b) The red triangle indicates the location of core CH2016 in Lake  
818 Chenghai, while green triangles indicate the locations of surface samples. (c) The

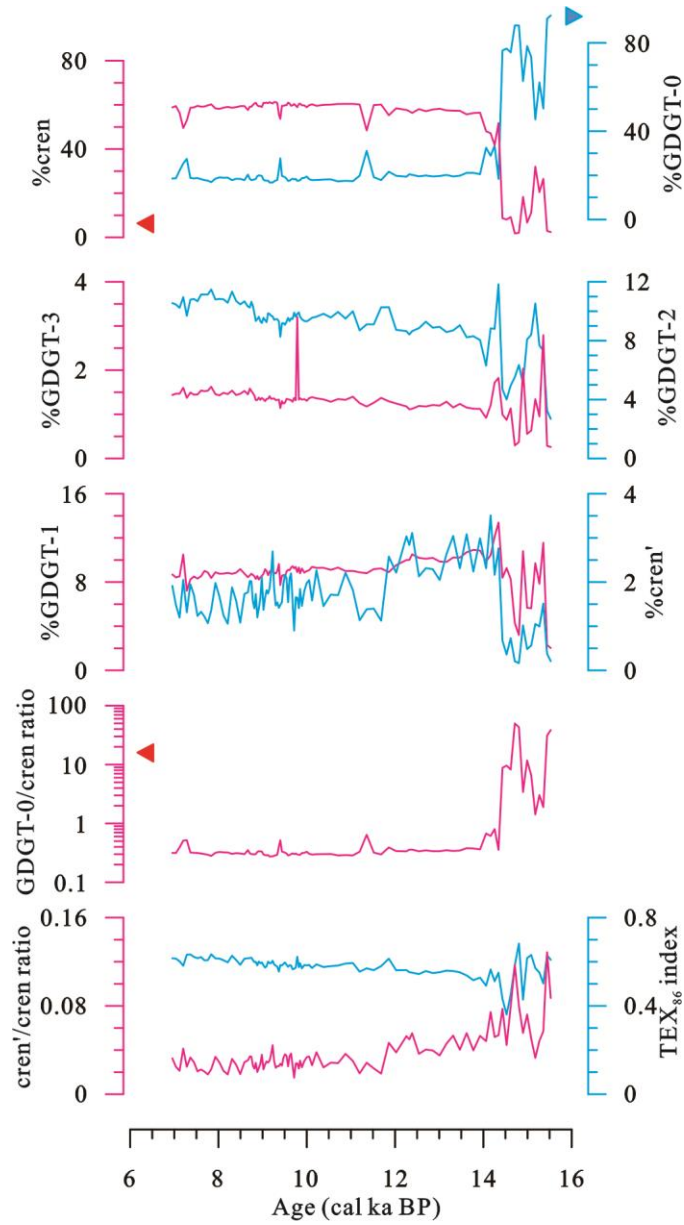
819 vertical variation of Lake Chenghai water temperature in March, May, July and  
820 October (Lu, 2018).



821

822 **Fig. 2.** (a) Age-depth model for the Lake Chenghai sediment core produced using  
823 Bacon software (Blaauw and Andres Christen, 2011) from Sun et al. (2019). Dotted  
824 lines indicate the 95% confidence range and the solid line indicates the weighted  
825 mean ages for each depth, error bars indicate the standard deviation range ( $2\sigma$ ) of the  
826 calibrated radiocarbon dates. (b) estimated sedimentation rate (Sun et al., 2019).

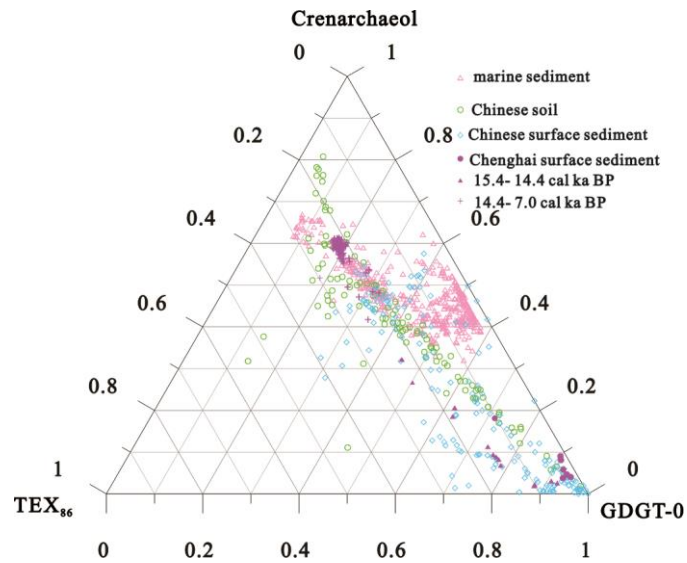
827



828

829 **Fig. 3.** Variations in the relative isoGDGT distribution and isoGDGTs-based proxies  
 830 of the Lake Chenghai sediment core. The triangles indicate the mean of surface  
 831 sediments.

832

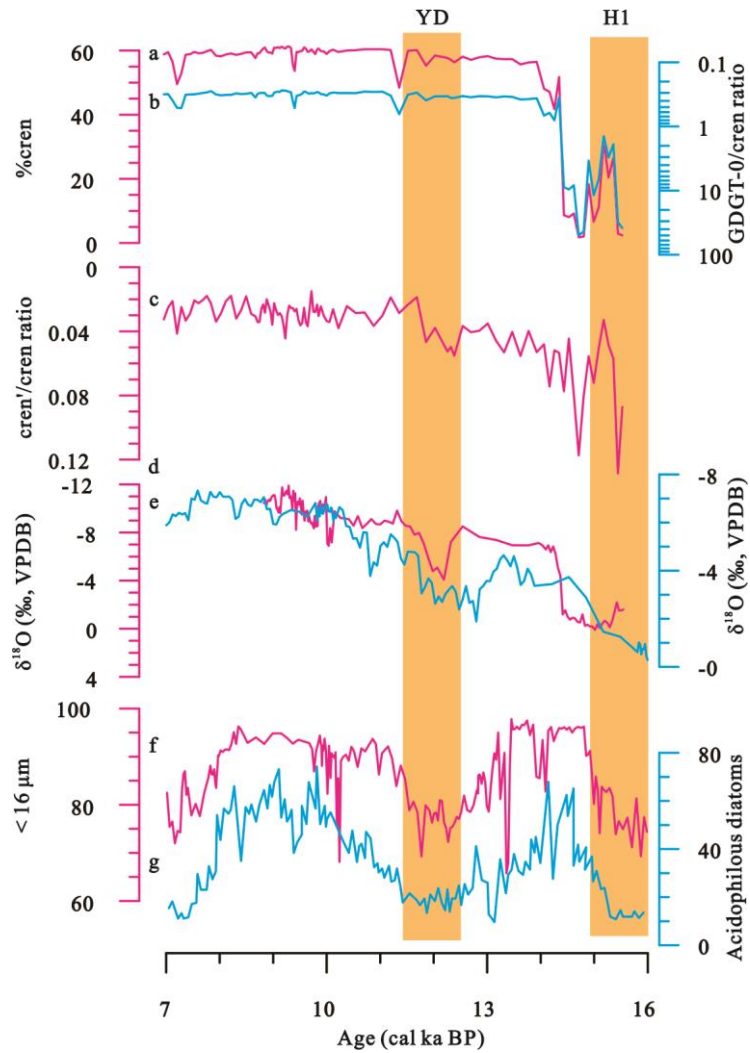


833

834 Fig. 4. Ternary diagram showing the distributions of GDGT-0, crenarchaeol, and  
 835 'TEX<sub>86</sub>' GDGTs in surface and core sediments from Lake Chenghai, global marine  
 836 sediments (Kim et al., 2010), published Chinese soils compiled by [Lao et al. \(2019\)](#),  
 837 and lacustrine surface sediments (Günther et al., 2014; Dang et al., 2016; Hu et al.,  
 838 2016; Li et al., 2016, 2019; Yao et al., 2019; Wang et al., 2020).

839

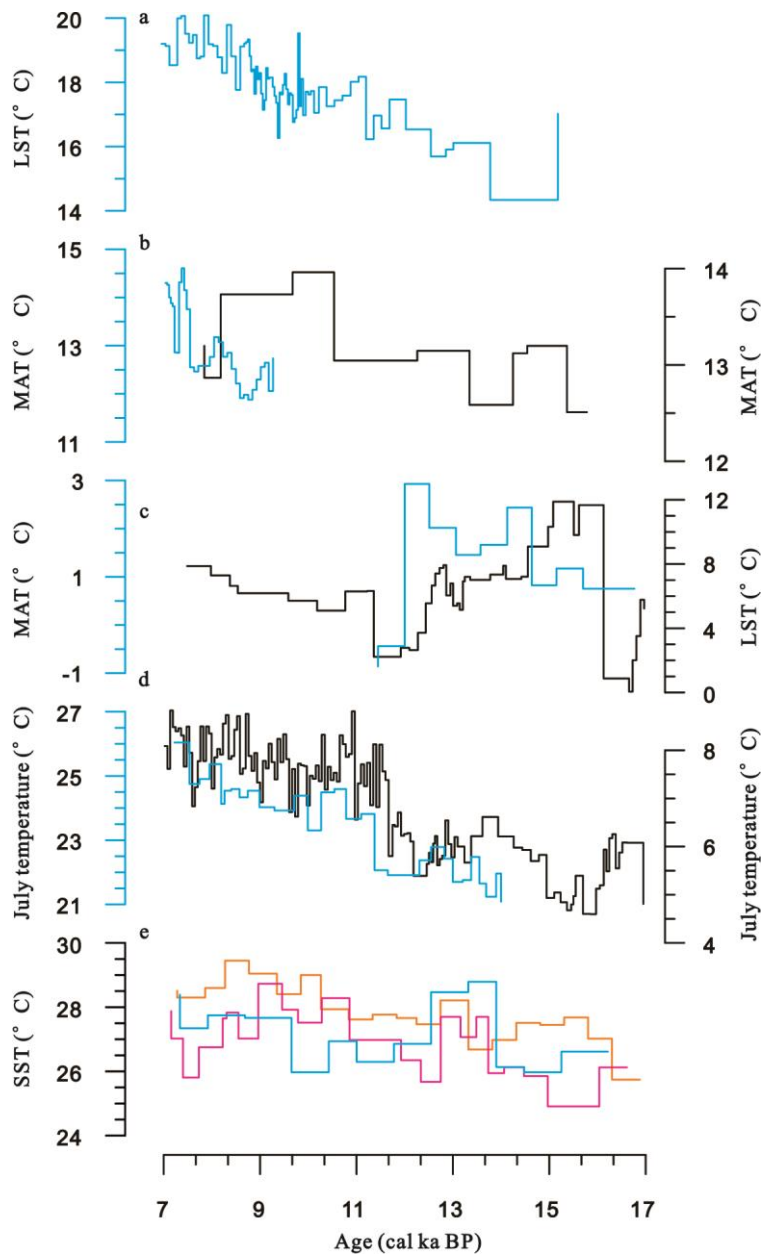




840

841 **Fig. 5.** Comparison of the isoGDGT-based lake-level record from Lake Chenghai (a-c)  
 842 with the  $\delta^{18}\text{O}$  record of carbonate finer in grain size than  $63\ \mu\text{m}$  from Lake Chenghai  
 843 (d, Sun et al., 2019), the stalagmite  $\delta^{18}\text{O}$  records from Mawmluh Cave in northeast  
 844 Indian (e, Dutt et al., 2015); grain-size and diatom record from Lake  
 845 Tengchongqinghai (f and g, Zhang et al., 2017; Li et al., 2018). The shading is utilised  
 846 to represent ‘cold’ events in the North Atlantic.

847



848

849 **Fig. 6.** A comparison of TEX<sub>86</sub>-based lake surface temperature of Lake Chenghai (a)  
 850 with other paleotemperature records. (b) mean annual temperature based on branched  
 851 GDGTs from Lake Ximenglongtan (blue line, Ning et al., 2019) and Lake  
 852 Tengchongqinghai (black line, Tian et al., 2019); (c) Alkenone-based mean annual  
 853 temperature at Lake Dangxiong (blue line, Ling et al., 2017), and TEX<sub>86</sub>-based lake  
 854 surface temperature of Nam Co from the southern Tibetan Plateau (black line,  
 855 Günther et al., 2015); (d) July temperature reconstructed from pollen record from  
 856 Lake Xingyun (blue line, Wu et al., 2018) and subfossil chironomids from Lake  
 857 Tiancai (black line, Zhang et al., 2017a, 2019);; and (e) sea surface temperatures in

858 the Andaman Sea and Bay of Bengal (Rashid et al., 2007; Govil and Naidu, 2011;  
859 Gebregiorgis et al., 2016).  
860